Large-amplitude quantum mechanics in polyatomic hydrides: II. A particle-on-a-sphere model for XH_n (n=4,5)

Michael P. Deskevich
JILA, University of Colorado, and Department of Chemistry and Biochemistry, University of Colorado, Boulder, Colorado 80309-0440, U.S.A.

Anne B. McCoy
Department of Chemistry, The Ohio State University, Columbus, Ohio 43210, U.S.A.

Jeremy M. Hutson
Department of Chemistry, University of Durham, South Road, Durham, DH1 3LE, United Kingdom

David J. Nesbitt
JILA, University of Colorado, National Institute of Standards and Technology and Department of Chemistry and Biochemistry, University of Colorado, Boulder, Colorado 80309-0440, U.S.A.

Abstract:

This paper describes the application of a relatively simple, but computationally tractable, "particles-on-a-sphere" (POS) model for quantum-mechanical calculation of large-amplitude, H atom dynamics in polyatomic hydrides (XH_n), based on radially relaxed, two-dimensional angular motion of H atoms on the surface of a sphere. This work focuses on systems with many degrees of freedom, i.e., XH_4 (8D) and XH_5 (10D), with corresponding molecular analogs of CH_4 and CH_5^+ and is applicable to rovibrationally excited states with $J \geq 0$. A pairwise-additive potential fit for CH_5^+ is presented which yields remarkable agreement with geometries, energies, barrier heights on the full-dimensional surface of Bowman and coworkers. Comparisons with experimental data and Diffusion Quantum Monte Carlo (DMC) methods test convergence for the POS model and provide insight into multidimensional quantum rovibrational dynamics. In particular, POS energy level patterns for a series of scaled CH_5^+ potentials indicate an *absence* of strong tunneling behavior, consistent with the highly delocalized wavefunctions, large

zero-point energies, and small interconversion barriers noted in the DMC studies of Bowman, McCoy and coworkers [J. Chem. Phys. 121, 4105 (2004)].

I. INTRODUCTION

The quantum mechanics of large-amplitude motion has been the focus of experimental and theoretical work for many decades. Advances in high-resolution rotational/vibrational spectroscopy have given much experimental evidence of large-amplitude dynamics in molecules and ions. In systems with few degrees of freedom, the exact quantum nuclear dynamics can be solved in full dimensionality, as in the well-studied triatomic systems (3D) such as H_2O[1-4]. Tetraatomic molecules require 6D and are significantly more challenging, but have been successfully tackled in a number of floppy systems, most notably the large-amplitude motion and tunneling inversion in ammonia[5-12] (NH_3) and hydronium ion[13-20] (H_3O^+). There have also been impressive advances in tetraatomic van der Waals complexes, such as the landmark 6D studies of HF and HCl dimers[21-24], as well as reduced-dimensionality extensions to H_2O dimer[25-28] using six-dimensional (6D) intermolecular coordinates with semirigid H_2O molecules. Even more challenging have been the full 9D calculations by Carrington[29-32], Bowman[33-35] and others for pentatomic species such as CH_4, which have successfully exploited sophisticated Lanczos methods in a tour de force calculation of rovibrational energies for $J > 0$ states.

As molecular systems increase in size and complexity, standard quantum-mechanical calculations rapidly become too expensive to permit treatment in full dimensionality, with a theoretical difficulty also increasing rapidly with total angular momentum, J. This is unfortunate, as some of the most interesting dynamics, such as

facile exchange of identical H atoms in protonated methane,[36,37] begin to emerge only in these larger systems. The addition of a single proton to relatively "rigid" methane, CH_4, creates the highly fluxional CH_5^+ molecule where simple Lewis octet bonding motifs do not apply. Five H atoms are connected by 4 electron pairs and require the presence of "three-center-two-electron bonds" ("3c-2e").[38] Such 3c-2e bonding motifs correspond to a special class of hypercoordinated carbocations, which are extremely important reactive intermediates in acid-catalyzed electrophilic reactions,[39,40] and for which CH_5^+ represents the simplest prototypic "superacid." CH_5^+ is also believed to be a key intermediate in the synthesis of polyatomic organic species in cold interstellar clouds,[41,42] which further motivates astrophysical interest in this simple, but spectroscopically elusive, molecular ion.

From a theoretical perspective, CH_5^+ is interesting because its relatively small size and high permutational symmetry make quantum-mechanical calculations of the potential energy surface computationally tractable, though still quite challenging. The most recent high-level calculations suggest three low-lying energy structures within about 1 kcal/mol of each other.[36,43-45] Furthermore, if zero-point energy is taken into account, these three configurations are all extensively sampled by the ground-state wave function. The barrier to rearrangement between these low-lying minima is considerably lower than the quantum zero-point vibrational energy, allowing facile intramolecular scrambling of the hydrogen atoms[43] to take place.

From a spectroscopic perspective, the highly fluxional, nonclassical nature of CH_5^+ begins to account for long-standing difficulties in interpreting its high-resolution spectrum. Despite its initial observation as a highly abundant ion in mass spectrometers

in the early 1950s,[46] optical detection and characterization of CH_5^+ eluded spectroscopists for another 50 years. The breakthrough came in 1999 from Oka and coworkers, who obtained a spectrum[47] in the CH-stretch region by exploiting velocity modulation methods. They made convincing arguments that the extensive, albeit rovibrationally unassigned, spectrum belonged predominantly to CH_5^+. Further progress has been made by Asvany and coworkers[48] in obtaining free electron laser IR action spectra of CH_5^+, which reveal broad vibrational structure from 3500 down to < 1000 cm^{-1}. Most recently, our group has obtained single-mode direct absorption IR spectra[49] in the 2820 -3050 cm^{-1} region, combining the two advantages of i) jet cooling and ii) high spectral resolution.

The need for help in the assignment process has led to considerable emphasis on direct calculation of near-IR spectra from first principles. However, despite intense theoretical efforts[36,43,50-62] directed toward CH_5^+ and the recent availability of a high-level potential surface, [44,45] high-resolution spectra based on fully converged exact rovibrational energy levels have proved extremely challenging to calculate. On the experimental side, delocalization of the wave function can result in rovibrational energy patterns profoundly perturbed from rigid-rotor expectations. From a theoretical perspective, the number of degrees of freedom for CH_5^+ is already too large to achieve converged quantum calculation of the rovibrational energy levels in full dimensionality for $J > 0$.

The particle-on-a-sphere (POS) model represents an alternative approximate method for calculating the energies and wave functions for molecules with large-amplitude motion in multiple degrees of freedom.[2,3,63] The spirit of the approach extends the pioneering work of Leitner, Natansan, Berry and coworkers, who first developed such

methods for triatomic systems (i.e., $n = 2$).[2,3] The essential idea is to decouple the fast X-H stretching coordinates adiabatically from the H-X-H bending coordinates, and thereby treat rotation and bending on an equivalent footing by expanding in a basis set of coupled spherical harmonics. This model has been extensively tested in a previous work on relatively "floppy" molecules (exhibiting large-amplitude bending dynamics) with rovibrational levels converged to spectroscopic accuracy for dihydride and trihydride species.[63]

However, the real potential advantage of such a POS approach lies in permitting one to move past $n = 3$ to systems of higher dimensionality. The present work addresses specifically $n = 4$ and 5, demonstrating strengths, challenges and limitations of the approach. The organization of this paper is as follows. Section II reviews the general theoretical background necessary to solve the POS problem efficiently, focusing explicitly on methods used in this work. Sections III and IV discuss applications of the particle-on-a-sphere model to $n = 4$ (XH_4) and $n = 5$ (XH_5) test systems. For $J = 0$, the POS methods are able to demonstrate convergence to DMC results even for relatively "stiff" species such as methane (CH_4), as well as to elucidate trends in energy level patterns for $J > 0$. Protonated methane (CH_5^+) proves more challenging, with fully converged results demonstrated for $J \geq 0$ only for scaled versions of the pairwise-additive potential, which nevertheless reveal a notable absence of tunneling splitting patterns. In Section V, we compare our $n = 5$ POS predictions with other large-amplitude theoretical results for CH_5^+. Concluding comments are given in Section VI.

II. THEORETICAL BACKGROUND

The POS model assumes a massive central atom ($m_X >> m_H$) and effectively averages over the high-frequency radial stretching of the X-H bond lengths, so that the resulting angular coordinates for each atom can be simply represented as 2D motion on a sphere.[63] This dimensionality reduction is achieved by adiabatically adjusting radial coordinates to minimize the energy as a function of the remaining 2*n* angular coordinates. The physical motivation in the case of CH_5^+ takes advantage of both the > 2-fold difference between the CH stretch and torsional/bending frequencies and the equivalent average CH bond lengths observed in trajectory calculations for H atoms with typical zero-point energies. The resulting Hamiltonian for the large-amplitude angular motion of *n* particles can then be simply expressed as

$$H_{POS} = \sum_{i=1}^{n} b\hat{j}_i^2 + \hat{V}(\Omega), \qquad (1)$$

where $\hat{j}_i$ is the angular momentum of the i^{th} hydrogen with respect to the stationary central atom, and *b* is the rotational constant for XH motion. The finite mass of the central atom is accounted for in the value of *b*. In addition to the terms shown in Eq. (1), there are cross terms in the kinetic energy operator that scale as the inverse of the mass of X. These are small compared to the single-particle terms and have been set to zero in the present treatment; this approximation is exact in the limit of infinite mass of the central atom. $\hat{V}(\Omega)$ is the potential describing the H atom interactions, where Ω is a 2*n*-dimensional vector of all H atom angular coordinates, of which 3 degrees of freedom are necessary to describe overall rotational motion.

One advantage of the POS approach is the lack of distinction between angular bending (2*n*-3) and end-over-end tumbling (3) degrees of freedom. Thus the solutions

treat vibration and rotation on an equivalent footing (i.e., there are no perturbative assumptions about the magnitude of Coriolis interactions). The method should work best in the limit of extreme large-amplitude quantum motion (e.g., CH_5^+) and relatively weak interparticle interactions. However, the corresponding cost of this equality with respect to rotational and vibrational coordinates is a much more rapid scaling of the variational problem with number of particles. Thus, although $n = 2$ (4D) and $n = 3$ (6D) systems are theoretically tractable from a variety of approaches, extension of the POS methods to $n = 4$ and 5 requires special techniques as described below.

A. Primitive and coupled basis sets

The goal of the POS model is to describe floppy molecules such as CH_5^+, where Coriolis coupling between overall rotation and H-X-H angular vibrations is large.[63] In the "floppy" limit, where the potential V(Ω) can be viewed as a perturbation of freely rotating XH bonds, one natural basis set in which to expand the Hamiltonian is simply a direct product of rigid-rotor functions,

$$\prod_{i=1}^{n} \left| j_i m_i \right\rangle . \tag{2}$$

The full *n*-particle Hamiltonian is diagonal in total $\hat{J}^2$ and $\hat{J}_Z$ so it is advantageous to transform this primitive basis set into an equivalent coupled representation[64] that permits matrix construction and diagonalization for each quantum number *J*. For increased speed in the potential matrix element evaluation, our choice of a coupled basis set for the XH_4 system is

$$\left| \left(\left(j_1 j_2 \right) j_{12} \left(j_3 j_4 \right) j_{34} \right) JM \right\rangle , \tag{3}$$

and for the XH_5 system is

$$\left|((j_1(j_2 j_3)j_{23})j_{123}(j_4 j_5)j_{45})JM\right\rangle. \quad (4)$$

In these expressions, j_i represents the angular momentum for the i^{th} particle, j_{ij} is the vector sum of j_i and j_j, parentheses denote the coupling order, and J and M represent the magnitude and Z projection of the total angular-momentum, respectively. In the absence of external fields, all M states for a given J are degenerate; thus M can be taken to be 0 for a further reduction by a factor of $2J + 1$ in the size of the Hamiltonian matrix. To create a basis set for a given J, the primitive free-particle angular momenta are restricted to $j_i = [0, j_{max}]$.

B. Basis set symmetrization and permutation inversion

To reduce computational effort, the Hamiltonian is block-diagonalized using group-theoretical methods.[65,66] This involves the use of permutation inversion theory[66] to create symmetry-adapted linear combinations (SALCs) of the coupled basis functions that transform according to each irreducible representation of permutation inversion symmetry group. The permutation inversion group for XH_4 is G_{48} (isomorphic to the direct product of the T_d point group with the inversion operation), with 10 irreducible representations: A_1^+, A_2^+, E^+, F_1^+, F_2^+, A_1^-, A_2^-, E^-, F_1^-, and F_2^-. For fermions with S=1/2, the nuclear spin weights are 5:1:3 for $A_1^{\pm}$:$E^{\pm}$:$F_2^{\pm}$, respectively. For XH_5, the permutation inversion group is G_{240}, characterized by 14 irreducible representations: A_1^+, A_2^+, G_1^+, G_2^+, H_1^+, H_2^+, I^+, A_1^-, A_2^-, G_1^-, G_2^-, H_1^-, H_2^-, and I^- with nuclear spin weights of 6:4:2 for $A_2^{\pm}$:$G_2^{\pm}$:$H_2^{\pm}$ symmetries,[61] respectively. Using projection operator techniques,[66] the coupled basis functions can be transformed into orthonormal SALCs of each irreducible

representation. For XH_5 in particular, these irreducible representations reflect high levels of intrinsic degeneracy, specifically E = 2, F = 3, G = 4, H = 5, and I = 6. By exploiting this degeneracy and including only one SALC for each irreducible representation,[67,68] one achieves a critical reduction in computational effort for matrix calculation and diagonalization.

C. Matrix element evaluation

Matrix element evaluation in the SALC basis set requires calculation of the integrals $\left\langle i\left|\hat{H}\right|i'\right\rangle$, which are expanded into sums of integrals over the direct product of each term in the SALCs. Creation of the symmetrized Hamiltonian matrix scales roughly as the 4th power, i.e. O(N^4), of basis set size. However, matrix element evaluation speed can be significantly improved when there are multiple symmetries into which SALCs can be distributed. Specifically, the matrix is reexpressed as $\mathbf{H}_\Gamma = \mathbf{S}_\Gamma^{\mathrm{T}} \cdot \mathbf{H}' \cdot \mathbf{S}_\Gamma$, where $\mathbf{H}'$ is the N_{coupled} x N_{coupled} unsymmetrized Hamiltonian, and $\mathbf{S}_\Gamma$ is a N_{coupled} x N_{SALC} matrix that transforms the coupled (unsymmetrized) basis functions into the SALC basis set. The advantage is that $\mathbf{S}_\Gamma$ is sparse (e.g., for XH_5, about 95% of the matrix elements are zero); thus computing terms in $\mathbf{H}'$ (too large to store for typical $N_{\mathrm{coupled}} \approx 75{,}000$), multiplied by nonzero terms in $\mathbf{S}_\Gamma$ is easily accomplished. Such a rearrangement of operations reduces to an O(N^3) algorithm, specifically N_{coupled} x N_{SALC} x $M_{\mathrm{SALC}} + N_{\mathrm{SALC}}^2$ x M_{SALC} matrix element evaluations, where M_{SALC} refers to the number of coupled basis states in a given SALC. This is about (N_{SALC} x M_{SALC})/($N_{\mathrm{coupled}} + N_{\mathrm{SALC}}$) times faster than the direct

product approach, resulting in a 50- to 100-fold increase in speed for large basis sets with many symmetries.

Evaluation of both the kinetic energy and potential energy matrix elements is analytic. Since the kinetic energy operator is diagonal in j_i^2, for XH_n, these matrix elements are simply

$$\left\langle i\left|\hat{T}\right|i'\right\rangle = b\sum_{k=1}^{n}\delta_{ii'}\,j_k\left(j_k+1\right), \tag{6}$$

where b is the internal X-H rotational constant and j_k is the angular momentum of the k^{th} X-H rotor. Calculation of the corresponding potential matrix elements is more challenging. To proceed, we consider the potential as a multicoordinate expansion, i.e.

$$V(\Omega)=\sum_{i<j}^{n}V^{(2)}(\Omega_i,\Omega_j)+\sum_{i<j<k}^{n}V^{(3)}(\Omega_i,\Omega_j,\Omega_k)+\sum_{i<j<k<l}^{n}V^{(4)}(\Omega_i,\Omega_j,\Omega_k,\Omega_l)+\ldots, \tag{7}$$

where each successive term represents a sum over all 2-coordinate, 3-coordinate, 4-coordinate, etc, contributions. As a surprisingly effective approximation, we restrict this expansion to the first term, i.e., linear combinations of potentials as a function of coordinates between pairs of particles,

$$V(\Omega)=\sum_{i<j}^{n}V^{(2)}\left(\gamma_{ij}\right), \tag{8}$$

where γ_{ij} is the H-X-H angle between the i^{th} and j^{th} hydrogen and $V^{(2)}$ is a sum of Legendre polynomials in γ_{ij}. As a result, the work required to calculate a potential matrix element grows as n^2 (the number of pairwise interactions for n particles), as opposed to Q^{2n} for numerical quadrature (with Q being the number of quadrature points per dimension). Furthermore, for a pairwise-additive potential expressed as a sum of Legendre polynomials, all the matrix elements can be calculated analytically via Clebsch-

Gordan angular momentum algebra and Percival-Seaton coefficients[63,69,70] as sums over 3-J and 6-J symbols. Thus one has gained the advantage of both an n^2 vs Q^{2n} scaling of integral evaluations and analytic evaluation of each matrix element. Although a pairwise-additive approximation to the potential was not essential for calculations in $n = 2$ and $n = 3$ systems, it proves crucial for extension to larger systems such as XH_4 and XH_5.

D. Rigid-body DMC

Direct comparison between the POS model and exact full-dimensional quantum-mechanical calculations was feasible for low J states of XH_2 and XH_3. For the more computationally demanding systems such as XH_5, exact full-dimensional quantum calculations for $J > 0$ are not available for benchmarking purposes. However, calculations for the ground rovibrational state ($J = 0$) are feasible with DMC methods, which scale much more favorably than variational methods for systems of high dimensionality (roughly linearly in $2n$). Thus, we can test the convergence of J=0 POS eigenvalues against DMC results, exploiting the "rigid body" formulation (RBDMC) to constrain the radial stretching coordinate for the diffusing $2n$-dimensional "walkers."[71-74]

III. FOUR PARTICLES ON A SPHERE (XH_4)

As the first challenge, we explore a 4-particle system, XH_4, with the POS method. To facilitate comparison with experiment, the HX rotor and H-X-H bending potential parameters (b_i = 16.63 cm^{-1} and γ_0=109.47°) are chosen to mimic the equilibrium structure of CH_4, with a pairwise additive $V^{(2)}(\gamma)$ term chosen to approximate the correct methane CH-bending frequencies (see Table I). This is a well-studied benchmark system,

tackled successfully with both high-level Lanczos/DVR methods by Carrington and coworkers[29-31] and sophisticated variational methods (MULTIMODE) by Bowman and coworkers.[34,35] The POS approach is not well suited for a molecule as "stiff" as CH_4, for which a more localized basis set offers advantages in speed and accuracy. Nevertheless, as seen below, we can achieve reasonably well converged J = 0 calculations with the POS method for a realistically stiff model of CH_4, where the Legendre polynomial coefficients (up to $l = 20$) used for the CH_4 potential expansion are listed in Table 1. To gain further insight into the rotational dynamics, we also converge calculations for a scaled angular potential, "softer" than methane by a multiplicative factor of α (i.e. $V_{\text{scaled}}(\gamma) = \alpha V^{(2)}(\gamma)$). In the stiff limit ($\alpha = 1$), the POS model of methane should yield a spherical top rotor with two ν_2 and ν_4 bending states corresponding to vibrations of E (≈ 1534 cm^{-1}) and F_2 (≈ 1306 cm^{-1}) symmetry, respectively. At higher resolution, the $(2J + 1)$ -fold degeneracy of the K levels of a rigid spherical top should be lifted by centrifugal interactions, leading to additional rotational fine structure for $J > 0$.

We first demonstrate the rate of convergence for $J = 0$ as a function of basis set size. Fig 1 plots the ground-state zero-point energy ($\Gamma = A_1^+$ symmetry) for realistically stiff (i.e.,$\alpha = 1$), J=0 CH_4 as obtained from the POS model for increasing values of $j_{\max}$. For comparison, also shown are the DMC predictions for the nodeless ground state, which corresponds to an exact calculation for $\Gamma = A_1^+$, J=0. Smooth, exponential energy convergence ($1/e$ decay rate of $\Delta j_{\max} \approx 2$) to DMC results is evident, even for relatively stiff systems which are far from ideal for the POS method. However, convergence using a coupled-rotor basis set also requires exponentially more time; for example, the $j_{\max} = 11$ calculations required about 1 month of CPU time to complete. By way of comparison,

Bowman and coworkers[34] use a more appropriate stiff-molecule basis set for CH_4 and achieve sub-wavenumber convergence of the vibrational frequencies with a basis set size ($\approx$ 4-10 x10^4) comparable to our POS with $j_{max} = 7$. Another point of comparison is provided by studies of Wang and Carrington,[30] who have performed calculations converged to spectroscopic accuracy for the bend manifold of CH_4, utilizing both much higher values of $j_{max} \approx 29$ and a correspondingly larger basis set (6.7 x 10^6).

Also of interest is how the POS model correctly captures the energy level patterns for rotationally excited states of CH_4. These more subtle effects require higher energy resolution, and thus scaling the potential by α to achieve comparable convergence with current computational capabilities. In Fig. 2, the vibrational ground state energies for J = 0 - 4 are shown as a function of j_{max}, based on $\alpha = 0.033$. By way of comparison, the dashed line in Fig. 3 represents the $J = 0$ DMC ground-state energy for the same potential; the inset illustrates eigenenergy agreement within the 1σ error of the DMC calculation. As expected, the basis set size increases rapidly with j_{max}; $N_{coupled}$ increases from 16,429 to 39,046 to 80,866 for j_{max} = 5, 6, and 7, respectively. If we empirically characterize convergence by the incremental decrease in POS eigenenergies for an increase in basis set size from j_{max}-1 to j_{max}, then $j_{max} = 7$ corresponds to a 0.001 cm^{-1} convergence for the lowest rotational state $J = 0$, with only slightly reduced (0.01 cm^{-1}) levels of convergence for excited rotational states J =1- 4. At this level of resolution, the rotational energies already exhibit spherical-top fine structure, with angular centrifugal distortion lifting the $(2J+1)$-fold degeneracy of the K levels for each J.

The progression of ground vibrational state energies for J=0-4 as a function of α is shown in Fig. 3, as the CH_4-like potential is increased from $\alpha = 0.0001$ (i.e., nearly

free-rotor limit) up to the stiffest value ($\alpha = 0.033$) that can be converged with j_{max}=7. In the $\alpha = 0.0001$ limit, the 4 individual C-H bonds rotate more or less independently, resulting in energy-level spacings characteristic of the C-H rotor constant. As the potential is stiffened, these states converge towards the $J(J+1)$ progression of energies characteristic of a spherical top, with the fine-structure splittings in Fig. 4 due to centrifugal bend-rotation coupling. Although the effective rotational spacing is only 20% above the experimental value (for $\alpha = 0.033$), the fine-structure splittings are ~500 times larger than expected. This implies that even for angular anisotropy scaled down by a factor of 30, the end-over-end tumbling structure for CH_4 is already reasonably well defined, with centrifugal fine-structure levels in the correct symmetry order and with qualitatively correct splitting ratios, though requiring larger basis sets (possibly as well as radial degrees of freedom) to converge on actual experimental values. Indeed, since the POS model neglects radial motion, $\alpha = 1$ calculations would provide an interesting opportunity to separate radial and angular contributions to the experimental centrifugal splittings.

Finally, in addition to comparison between POS and experimental rotational energies in the ground vibrational state, we can also inspect the low-frequency vibrational states of methane (ν_2,E and ν_4,F_2) in the rotationless $J = 0$ level (see Fig. 4). Since it was possible to use a larger j_{max} for $J = 0$ calculations, these energies have been converged with a potential ($\alpha = 0.33$) that is 10-fold stiffer than for $J > 0$, but still somewhat short of the full methane potential. As the potential approaches the full methane stiffness, the energies of the ν_2,E and ν_4,F_2 vibrations increase monotonically towards experimental values,[75] with the order of the ν_2,E and ν_4,F_2 vibrations maintained even for substantially

floppier potentials. Similar qualitative agreement is noted for states with two quanta of bending energy, as shown in Fig. 5 for $2\nu_2$,A_1+E, $\nu_2+\nu_4$,F_1+F_2, and $2\nu_4$,A_1+E+F_2. As for the calculations presented earlier, the ordering of the dyads is correctly predicted, with the vibrational fine-structure splittings decreasing as the potential stiffens.

IV. FIVE PARTICLES ON A SPHERE (XH_5)

As mentioned above, the POS model is not well suited to a relatively stiff molecule such as CH_4, which can be treated more quantitatively with other methods. However, for floppier systems the POS model offers a more favorable scaling with n, and is thus promising for application to challenging fluxional systems such as CH_5^+. We first characterize the individual C-H rotor with b = 12.81 cm^{-1}, consistent with expectation values of the C-H bond length from full-dimensional DMC calculations, for which the five CH bond lengths are considered in addition to the ten angular coordinates.[45,76] For the remainder of this paper, therefore, we will describe such full-dimensional calculations as 15D, with reduced-dimensional calculations in the ten angular coordinates referred to as 10D. As discussed earlier, a pairwise-additive potential with each term expressed as a sum of Legendre functions can be exploited for analytic evaluation of the potential operator matrix. To take advantage of this, the full CH_5^+ potential must be expressed as a sum of pairwise potentials.

As the first step, the 15D MP2/cc-pVTZ potential of Bowman[45] is adiabatically relaxed in the "fast" CH stretch coordinate to create a 10D potential that depends only on the relative angular coordinates. This process also automatically ensures identical angular geometries and energies of all critical points for the full 15D and reduced 10D potential.

The resulting critical point geometries as a function of intrinsic reaction coordinate (IRC) are shown in Fig. 5. The minimum energy structure of CH_5^+ on the Bowman potential is of C_s symmetry, consisting of what looks like an elongated H_2 perched on top of a CH_3^+ structure. However, at the wave function level, there is rapid quantum exchange of hydrogen atoms between between the "H_2" and "CH_3" moieties, resulting in delocalization of each of the H atoms between the 120 equivalent geometries separated by low barriers. For example, the H_2 (or CH_3^+) moiety can "rotate" through a C_s transition state (E = 43 cm^{-1}) or "flip" H's between H_2 and CH_3^+ through a slightly higher C_{2v} transition state (E = 192 cm^{-1}). Analysis of the potential shows that pathways involving "flip" and "rotation" saddle points exist between any pair of the 120 minima on the CH_5^+ surface.

The second step is to represent the 10D potential by a sum of pairwise potentials, which is achieved by least-squares fitting 10,000 randomly selected points with energies below 1,000 cm^{-1}. The energies and angular geometries of these points are then fit to a sum of pairwise terms, with each term described by a sum of Legendre functions. (See Table 1 for a list of the coefficients). Of particular relevance is a comparison between 10D and pairwise potentials for the "flip" and "torsion" reaction paths and critical points between C_{2v} and C_s minima. Such a comparison is shown in Fig. 5 for (i) the 10D radially relaxed version of the full 15D Bowman potential and (ii) the pairwise fit potential. Given the simple nature of the pairwise-additive approximation, the agreement between the 10D and pairwise critical points is truly remarkable. Similar accuracy is also demonstrated in Fig. 5 for both the 10D potential and the pairwise fit along the C_s

(internal rotation) and C_{2v} ("H_2 flip") reaction paths. Again, the differences between the 10D potential and pairwise fit are surprisingly small.

DMC methods provide one additional opportunity to test the validity of the pairwise approximation for both full 15D and 10D radially relaxed potentials. Specifically, DMC is able to calculate the ground state *wave function* at all three levels of dimensionality (POS, 10D and 15D), each of which can then be projected onto the γ coordinate (where γ is the angle between any two particles) for more quantitative comparison. The results are summarized in Fig. 6, which again reveals surprisingly good agreement. The main peak in each wave function near 110^o corresponds to unresolved features due to i) the H-C-H angles in the CH_3^+ motif, and ii) the angle between one of the H_2 hydrogens and a CH_3^+ hydrogen, with the smaller shoulder near 60^o reflecting contributions from iii) the smaller H-C-H central angle between the H_2 hydrogens. Treatments at the POS, 10D and 15D levels yield nearly identical H-C-H interangular distributions, indeed indistinguishable within statistical uncertainty of the DMC calculation. This clearly indicates that a relatively simple pairwise potential can capture H-C-H angular correlations at a remarkably quantitative level.

In analogy to our strategy for the $n = 4$ particle problem, we first look for convergence in the ground state ($J = 0$, A_1^+) eigenenergy for CH_5^+ $n = 5$ particle POS calculations as a function of basis set size. The results for the fully anisotropic potential (i.e. $\alpha = 1$) are summarized in Fig. 7, which demonstrates steady convergence with respect to j_{max}. For comparison, we also show the DMC results as an exact lower bound at large j_{max} to the POS variational treatment, with single processor CPU times associated with each j_{max} calculation listed by each point. Although convergence toward the DMC

result is clearly evident, the zero-point energy is still overestimated at $j_{max} = 7$ by ≈ 30% for the full potential anisotropy. Extension to higher j_{max} will be necessary for improved levels of convergence, which may profit both by parallelization of the matrix element calculation routines and possibly by incorporation of the Lanczos methods of Wang and Carrington.[29-31,77,78]

The POS convergence as a function of potential anisotropy is summarized in Fig 8, where the pairwise 10D fit of the full 15D Bowman CH_5^+ surface is stiffened from $\alpha = 0.0001$ up to $\alpha = 1$. Zero-point energy (solid line) from the POS model is compared with converged DMC energies and uncertainties for 10D pairwise (solid circles) and nonpairwise (open squares) potentials. Agreement between POS eigenvalue predictions for pairwise and exact 10D results is excellent at low α. This comparison illustrates the degree of convergence of the POS calculations at a *spectroscopic* level as a function of potential stiffness. Up to $\alpha = 0.01$, the ground-state $J = 0$ energies are converged to of order 1 cm^{-1} for $j_{max} = 5$. For $\alpha = 0.1$, convergence for $J = 0$ is approximately 10 cm^{-1}, which is comparable to $j_{max} = 5$ results for J=1 and 2 rotationally excited states at $\alpha = 0.01$. Finally, the differences between rovibrational energy levels converge faster with j_{max} than the absolute energies themselves, as is evident from a close inspection of the data.

V. DISCUSSION

The theoretical issues posed by CH_5^+ have been addressed by numerous *ab initio* potential surface investigations over the years; however, efforts to predict detailed rovibrational energy levels for a given potential surface have proved even more

challenging. Landmark work by Bunker and co-workers,[61] using a rotation-contortion Hamiltonian,[60] has been used to predict the $J = 0 \leftarrow 1$ microwave spectrum of CH_5^+, exploiting symmetry correlations between the two extremes associated with rigid C_s and C_{2v} potential minima. In this rotation-contortion approach, considerable effort was made to calculate energies for states of nonzero statistical weight for a number of different flip and torsion rearrangement barriers, based on a Hamiltonian which adiabatically separates *one* large-amplitude internal contortional mode from the remaining 11 "fast" vibrational modes. The Hamiltonian is a sum of H^{rot} (end-over-end tumbling of the molecule), H^{τ} (motion along the contortion degree of freedom), and $H^{rot,\tau}$ (coupling between tumbling and contortion), with all coupling between the "fast" vibrations and overall rotation neglected. The POS model provides an alternative formulation that neglects the contributions from the 5 "fastest" CH-stretching vibrations, but does include the 7 low-energy bending vibrations and allows full coupling of these vibrations to end-over-end tumbling of the CH_5^+ molecule. This motivates a brief comparison of POS predictions with the rotation-contortion results, with an eye toward establishing additional insights into the dynamical trends anticipated for CH_5^+.

The 53.9 cm^{-1} torsional and 213.9 cm^{-1} flip barriers from least-squares pairwise fits to the full 15D Bowman surface (i.e., $\alpha = 1$) most closely approximate the reduced-dimensional rotation-contortion model[61] barriers of 50 cm^{-1} and 200 cm^{-1}, respectively. The $\alpha = 1$ POS CH_5^+ calculations are not converged; we therefore compare converged POS eigenenergies for the lowest $J = 0$ states of nonzero nuclear spin statistical weight as a function of stiffness. Fig. 9 presents results for $\alpha = 0.0001$, $\alpha = 0.001$, $\alpha = 0.01$ and $\alpha = 0.1$, for which the DMC calculations (A_1^+) indicate absolute convergence levels of

approximately, 0.01 cm^{-1}, 0.1 cm^{-1}, 1 cm^{-1} and 10 cm^{-1}, respectively. The corresponding J=0 energy levels obtained from the full rotation-contortion model (with 200 cm^{-1} flip and 50 cm^{-1} torsional barriers) for the same series of nuclear-spin symmetry states are also shown in Fig. 9. All energies are reported as splittings with respect to the lowest nuclear spin allowed G_2^- state, which are converged better than the absolute energies themselves.

The free-rotor energy patterns observed in Fig. 9 at low α evolve to more complex internal-rotor splitting patterns with increasing potential stiffness. A monotonically increasing trend in rotor energy spacing with stiffness is clearly evident, with an energy ordering in the lowest several states largely maintained with respect to α. The converged energy level differences for the *stiffest* POS calculations ($\alpha = 0.1$) suggest significant differences with the rotation-contortion model. Specifically, the POS results indicate a notable absence of tunneling splittings as well as a less defined clustering of energy levels into internal-rotor K manifolds than predicted by the 1D rotation-contortion model. Such a lack of apparent tunneling behavior would be entirely consistent with the delocalized wavefunctions, large zero-point energies, and small interconversion barriers previously noted in DMC studies of CH_5^+ by McCoy, Bowman and coworkers.[45,79] Furthermore, the level splittings exhibit a relatively soft dependence on the potential stiffness. Such behavior would also be more consistent with large-amplitude internal-rotor behavior than with localized vibrational motion, for which the spacings would presumably continue to grow with the square root of the potential stiffness, $\alpha^{1/2}$. Most importantly, trends in these energy level patterns with α already provide useful insight

into the highly delocalized nature of the excited-state CH_5^+ wavefunctions, as opposed to a scenario of more localized vibrational states tunneling between multiple minima.

Wang and Carrington have very recently succeeded in performing a landmark full-dimensional study on the J=0 vibrational levels of CH_5^+, with results to be published elsewhere.[77] In this work, they first separately solve the 5D CH stretch subsystem and the 7D bending subsystem. They then couple the two halves of the Hamiltonian to obtain energies in 12D, restricted to J=0. In light of the relatively slow dependence of POS splittings on α, it is tempting to compare trends in the converged results for $\alpha < 1$ with results obtained by Wang and Carrington for the 7D bending subsystem at full anisotropy. Unfortunately the two calculations employ different potentials. Specifically, Wang and Carrington used a slightly modified version of a later global surface for CH_5^+, reported by Bowman and co-workers[79], for which the electronic energies were calculated at the coupled-cluster level of theory [CCSD(T)]. This surface has isomerization barriers of 29 and 341 cm^{-1}. As mentioned above, the PWA potential used in the present work has corresponding barriers of 54 and 214 cm^{-1}, in good agreement with the barriers on the MP2 surface on which it is based.[45] Given the expected sensitivity of the energy levels to, in particular, the lower energy barrier, and the nearly factor of two difference in the heights of this barrier, a quantitative comparison does not seem appropriate at this stage, particularly as our numbers are based on scaling of the potential anisotropy. On the other hand, it will ultimately prove interesting to see how sensitive these energy spacings are to the height of the barriers.

As a final note, we can estimate the value of j_{max} necessary to achieve convergence at $\alpha = 1$ for CH_5^+ in the POS model. In Fig. 10a, the RBDMC wave

function is projected onto the γ coordinate for α = 0.001, 0.01, 0.1, and 1. As expected, the α = 0.001 wave function is essentially identical to the sin γ Jacobian expected for free-particle motion. More structure in the wave function appears as α is increased, requiring more angular flexibility in the multidimensional wave function. A simple metric of the j_{max} value required to converge the α = 1 POS calculation is therefore obtained by expanding the corresponding 1D DMC pair correlation function in the H-C-H angle γ as a sum of Legendre functions $P_l(\gamma)$ and probing the degree of convergence with respect to l. The physical notion is that angular flexibility in a sum of Legendre functions with $l \leq j_{max}$ mirrors the angular flexibility and thus convergence behavior for a sum of SALCs with the same j_{max}. Fig. 10b displays the 1D DMC wavefunction obtained with several Legendre polynomial expansions, indicating a rapid convergence with increasing j_{max}.

More quantitatively, if the expectation value of the energy for a 1D rotor in the α = 1 pairwise potential is calculated using the wave functions expanded in Legendre polynomials of increasing order (j_{max}), the convergence with respect to j_{max} should mirror the number of Legendre functions required to represent the 1D wave function accurately. As illustrated in Table 5, POS ground state CH_5^+ α = 1 energy convergence to the DMC value should be feasible at the ≈ 1% level with coupled rotor basis sets including up to $j_{max} \approx 9$.

VI. SUMMARY AND CONCLUSION

This paper presents results from a conceptually simple yet flexible approach for the approximate quantum treatment of large-amplitude motion in systems with many

degrees of freedom and $J > 0$. The particle-on a-sphere (POS) method takes advantage of the approximate independence of the XH bond length on angle to motivate a reduced-dimensionality treatment of *n* hydrogens, adiabatically relaxed in the radial coordinate. Consistent with this physical picture, the basis set for expanding the Hamiltonian is designed around symmetry-adapted linear combinations of coupled free-rotor states with well defined *J* and permutation inversion symmetry. Convergence for 4-particle systems such as CH_4 is possible with POS methods, and already reveals interesting dynamical behavior as a function of *J* in terms of centrifugally-induced lifting of the $2J+1$-fold degeneracies of the rotational levels for a spherical top.

In order to extend these POS methods to even more challenging $n=5$ particle systems, we have developed a pairwise-additive 10D potential for CH_5^+, based on adiabatic relaxation of the CH bond lengths and least-squares fitting of the full 15D potential by Bowman and coworkers[79] to a Legendre expansion in H-C-H bond angle. This relatively simple potential reproduces the equilibrium/transition state geometries, barrier heights and flip/torsion reaction paths remarkably well, which should prove of significant utility in other reduced-dimensionality treatments of CH_5^+. To date, fully converged results for CH_5^+ are obtainable with the POS model only for a scaled version of this potential. Nevertheless, the energy level patterns observed for such model potentials exhibit trends that begin to provide insight into the rotational dynamics of these complicated systems. Specifically, the results as a function of potential stiffness already signal the *absence* of tunneling splittings and other indications of a strong tunneling regime. Indeed, this is entirely consistent with DMC results of Bowman and McCoy[45] that reveal zero-point energies significantly higher than transition state barriers and a

widely delocalized ground state wave function spread over multiple minima. A more predictive understanding of *rotational* level patterns in highly fluxional systems such as CH_5^+ will undoubtedly profit from further development of reduced dimensionality approaches such as the POS model, which offer access to J> 0 quantum calculations extremely challenging to achieve currently in full dimensionality.

ACKNOWLEDGEMENT

This work has been supported by funds from the National Science Foundation, with additional computational support from the Air Force Office of Scientific Research and the Ohio Supercomputer Center. The authors would also like to thank Professor Joel Bowman for providing the source code for the 15D CH_5^+ potential energy surface, and Professor Tucker Carrington and Dr. Xiaogang Wang for sharing their recent results on CH_5^+ ($J = 0$) prior to publication.

References

[1] O. L. Polyansky, P. Jensen, and J. Tennyson, J. Chem. Phys. **105**, 6490 (1996).

[2] G. A. Natanson, G. S. Ezra, G. Delgado-Barrio, and R. S. Berry, J. Chem. Phys. **81**, 3400 (1984).

[3] G. A. Natanson, G. S. Ezra, G. Delgado-Barrio, and R. S. Berry, J. Chem. Phys. **84**, 2035 (1986).

[4] D. M. Leitner, J. E. Hunter, G. A. Natanson, R. S. Berry, P. Villarreal, and G. Delgado-Barrio, J. Chem. Phys. **94**, 5917 (1991).

[5] V. Spirko, J. Mol. Spectrosc. **101**, 30 (1983).

[6] S. Urban, R. Dcunha, K. N. Rao, and D. Papousek, Can. J. Phys. **62**, 1775 (1984).

[7] S. L. Coy and K. K. Lehmann, Spectroc. Acta Pt. A-Molec. Biomolec. Spectr. **45**, 47 (1989).

[8] V. Spirko and W. P. Kraemer, J. Mol. Spectrosc. **133**, 331 (1989).

[9] S. Urban, N. Tu, K. N. Rao, and G. Guelachvili, J. Mol. Spectrosc. **133**, 312 (1989).

[10] I. Kleiner, G. Tarrago, and L. R. Brown, J. Mol. Spectrosc. **173**, 120 (1995).

[11] I. Kleiner, L. R. Brown, G. Tarrago, Q. L. Kou, N. Picque, G. Guelachvili, V. Dana, and J. Y. Mandin, J. Mol. Spectrosc. **193**, 46 (1999).

[12] C. Cottaz, I. Kleiner, G. Tarrago, L. R. Brown, J. S. Margolis, R. L. Poynter, H. M. Pickett, T. Fouchet, P. Drossart, and E. Lellouch, J. Mol. Spectrosc. **203**, 285 (2000).

[13] J. Tang and T. Oka, J. Mol. Spectrosc. **196**, 120 (1999).

[14] D. J. Liu, T. Oka, and T. J. Sears, J. Chem. Phys. **84**, 1312 (1986).

[15] P. B. Davies, S. A. Johnson, P. A. Hamilton, and T. J. Sears, Chem. Phys. **108**,

335 (1986).

[16] M. H. Begemann and R. J. Saykally, J. Chem. Phys. **82**, 3570 (1985).

[17] M. Gruebele, M. Polak, and R. J. Saykally, J. Chem. Phys. **87**, 3347 (1987).

[18] H. Petek, D. J. Nesbitt, J. C. Owrutsky, C. S. Gudeman, X. Yang, D. O. Harris, C. B. Moore, and R. J. Saykally, J. Chem. Phys. **92**, 3257 (1990).

[19] M. Araki, H. Ozeki, and S. Saito, Mol. Phys. **97**, 177 (1999).

[20] M. Araki, H. Ozeki, and S. Saito, J. Chem. Phys. **109**, 5707 (1998).

[21] D. H. Zhang, Q. Wu, J. Z. H. Zhang, M. Vondirke, and Z. Bacic, J. Chem. Phys. **102**, 2315 (1995).

[22] G. W. M. Vissers, G. C. Groenenboom, and A. van der Avoird, J. Chem. Phys. **119**, 277 (2003).

[23] Y. H. Qiu, J. Z. H. Zhang, and Z. Bacic, J. Chem. Phys. **108**, 4804 (1998).

[24] Y. H. Qiu and Z. Bacic, J. Chem. Phys. **106**, 2158 (1997).

[25] P. Eggert, A. Viel, and C. Leforestier, Comput. Phys. Commun. **128**, 315 (2000).

[26] N. Goldman, R. S. Fellers, C. Leforestier, and R. J. Saykally, J. Phys. Chem. A **105**, 515 (2001).

[27] F. N. Keutsch, N. Goldman, H. A. Harker, C. Leforestier, and R. J. Saykally, Mol. Phys. **101**, 3477 (2003).

[28] N. Goldman, C. Leforestier, and R. J. Saykally, J. Phys. Chem. A **108**, 787 (2004).

[29] X. G. Wang and T. Carrington, J. Chem. Phys. **119**, 101 (2003).

[30] X. G. Wang and T. Carrington, J. Chem. Phys. **118**, 6946 (2003).

[31] X. G. Wang and T. Carrington, J. Chem. Phys. **121**, 2937 (2004).

[32] X. G. Wang and T. Carrington, J. Chem. Phys. **123** (2005).

[33] Z. Xie, J. M. Bowman, and X. B. Zhang, J. Chem. Phys. **125**, 133120 (2006).

[34] J. Y. Wu, X. C. Huang, S. Carter, and J. M. Bowman, Chem. Phys. Lett. **426**, 285 (2006).

[35] S. Carter and J. M. Bowman, J. Phys. Chem. A **104**, 2355 (2000).

[36] P. R. Schreiner, S. J. Kim, H. F. Schaefer, and P. V. Schleyer, J. Chem. Phys. **99**, 3716 (1993).

[37] H. Muller and W. Kutzelnigg, Phys. Chem. Chem. Phys. **2**, 2061 (2000).

[38] D. Marx and M. Parrinello, Nature **375**, 216 (1995).

[39] G. A. Olah, N. Hartz, G. Rasul, and G. K. S. Prakash, J. Am. Chem. Soc. **117**, 1336 (1995).

[40] G. A. Olah and G. Rasul, Accounts Chem. Res. **30**, 245 (1997).

[41] E. Herbst, S. Green, P. Thaddeus, and W. Klemperer, Astrophys. J. **503** (1977).

[42] D. Talbi and R. P. Saxon, Astron. Astrophys. **261**, 671 (1992).

[43] H. Muller, W. Kutzelnigg, J. Noga, and W. Klopper, J. Chem. Phys. **106**, 1863 (1997).

[44] A. Brown, B. J. Braams, K. Christoffel, Z. Jin, and J. M. Bowman, J. Chem. Phys. **119**, 8790 (2003).

[45] A. Brown, A. B. McCoy, B. J. Braams, Z. Jin, and J. M. Bowman, J. Chem. Phys. **121**, 4105 (2004).

[46] V. L. Tal'rose and A. K. Lyubimova, Dokl. Akad. Nauk SSSR **86**, 909 (1952).

[47] E. T. White, J. Tang, and T. Oka, Science **284**, 135 (1999).

[48] O. Asvany, P. Kumar, B. Redlich, I. Hegemann, S. Schlemmer, and D. Marx,

Science **309**, 1219 (2005).

[49] X. C. Huang, A. B. McCoy, J. M. Bowman, L. M. Johnson, C. Savage, F. Dong, and D. J. Nesbitt, Science **311**, 60 (2006).

[50] J. S. Tse, D. D. Klug, and K. Laasonen, Phys. Rev. Lett. **74**, 876 (1995).

[51] A. Gamba, G. Morosi, and M. Simonetta, Chem. Phys. Lett. **3**, 20 (1969).

[52] G. A. Olah, G. Klopman, and R. H. Schlosberg, J. Am. Chem. Soc. **91**, 3261 (1969).

[53] W. T. A. M. Van der Lugt and P. Ros, Chem. Phys. Lett. **4**, 389 (1969).

[54] W. A. Lathan, W. J. Here, and J. A. Pople, J. Am. Chem. Soc. **93**, 808 (1971).

[55] P. R. Schreiner, Angew. Chem.-Int. Edit. **39**, 3239 (2000).

[56] A. Komornicki and D. A. Dixon, J. Chem. Phys. **86**, 5625 (1987).

[57] W. Klopper and W. Kutzelnigg, J. Phys. Chem. **94**, 5625 (1990).

[58] S. J. Collins and P. J. Omalley, Chem. Phys. Lett. **228**, 246 (1994).

[59] M. Kolbuszewski and P. R. Bunker, J. Chem. Phys. **105**, 3649 (1996).

[60] A. L. L. East, M. Kolbuszewski, and P. R. Bunker, J. Phys. Chem. A **101**, 6746 (1997).

[61] P. R. Bunker, B. Ostojic, and S. Yurchenko, J. Mol. Struct. **695**, 253 (2004).

[62] G. A. Olah, Angew. Chem. Int. Ed. Engl. **34**, 1393 (1995).

[63] M. P. Deskevich and D. J. Nesbitt, J. Chem. Phys. **123**, 084304 (2005).

[64] R. N. Zare, *Angular Momentum: Understanding Spatial Aspects in Chemistry and Physics*. (John Wiley & Sons, New York, 1988).

[65] F. A. Cotton, *Chemical Applications of Group Theory*, 3rd ed. (Wiley, New York, 1990).

[66] P. R. Bunker and P. Jensen, *Molecular Symmetry and Spectrosopy*, 2nd ed. (NRC Research Press, Ottawa, 1998).

[67] I. G. Kaplan, *Symmetry of Many-electron Systems*. (Academic Press, New York, 1975).

[68] J. F. Cornwell, *Group Theory in Physics: An Introduction*. (Academic Press, San Diego, 1987).

[69] J. M. Hutson, in *Advances in Molecular Collision Dynamics*, edited by J. M. Bowman and M. A. Ratner (JAI Press, 1990), Vol. 1A, p. 1.

[70] A. M. Arthurs and A. Dalgarno, Proc. Royal Soc. London Series A-Mathematical and Physical Sciences **256**, 540 (1960).

[71] V. Buch, J. Chem. Phys. **97**, 726 (1992).

[72] J. B. Anderson, J. Chem. Phys. **63**, 1499 (1975).

[73] M. A. Suhm and R. O. Watts, Phys. Rep.-Rev. Sec. Phys. Lett. **204**, 293 (1991).

[74] A. Vegiri, M. H. Alexander, S. Gregurick, A. B. McCoy, and R. B. Gerber, J. Chem. Phys. **101**, 2577 (1994).

[75] G. Herzberg, *Infrared and Raman Spectra of Polyatomic Molecules*. (D. Van Nostrand Company, Inc, New York, 1945).

[76] A. B. McCoy, B. J. Braams, A. Brown, X. C. Huang, Z. Jin, and J. M. Bowman, J. Phys. Chem. A **108**, 4991 (2004).

[77] X. G. Wang and T. Carrington (private communication).

[78] X. G. Wang and T. Carrington, J. Chem. Phys. **114**, 1473 (2001).

[79] Z. Jin, B. J. Braams, and J. M. Bowman, J. Phys. Chem. A **110**, 1569 (2006).

[80] P. R. Bunker, J. Mol. Spectrosc. **176**, 297 (1996).

TABLE 1. Particle-on-a-sphere (POS) Legendre coefficients for expansion of the CH_4 and CH_5^+ potentials in a pairwise-additive approximation ($\alpha = 1$).

l	CH_4 a_l (cm^{-1})	CH_5^+ a_l (cm^{-1})
0	3890.27	4190.442
1	5007.02	3060.609
2	6929.86	14790.49
3	17.7851	1821.198
4	1540.04	9008.753
5	26.7693	2796.952
6	673.460	5626.363
7	37.8839	1216.296
8	362.223	2174.996
9	47.7746	238.9801
10	211.010	381.5193
11	57.5209	
12	123.637	
13	67.0757	
14	66.9194	
15	0.01038	
16	26.8277	
17	-0.01821	
18	-3.40294	
19	94.3927	
20	-27.3240	

TABLE 2. CH_5^+ critical point geometries and energies for the full 15D and 10D pairwise fit potentials.

	C_s Min		C_s ‡		C_{2v} ‡	
	15D	Pairwise	15D	Pairwise	15D	Pairwise
(θ_1,ϕ_1)	(0.00,0.00)	(0.00,0.00)	(0.00,0.00)	(0.00,0.00)	(0.00,0.00)	(0.00,0.00)
(θ_2,ϕ_2)	(75.70,0.00)	(75.52,0.00)	(108.55,-25.41)	(108.36,-25.39)	(61.76,0.00)	(61.89,0.00)
(θ_3,ϕ_3)	(124.47,0.00)	(124.21,0.00)	(108.55,25.41)	(108.36,25.39)	(123.52,0.00)	(123.79,0.00)
(θ_4,ϕ_4)	(108.50,-114.13)	(108.28,-114.28)	(115.62,-119.04)	(116.00,-118.03)	(103.25,-116.00)	(103.18,-115.99)
(θ_5,ϕ_5)	(108.50,114.13)	(108.28,114.28)	(115.62,119.04)	(116.00,118.03)	(103.25,116.00)	103.18,115.99)
E (cm^{-1})	0	-1.9	43.3	53.9	192.5	213.9

TABLE 3: Zero-point energies of CH_5^+ as a function of scale factor α, calculated with i) DMC/non-pairwise 10D potential, ii) DMC/pairwise potential, and iii) POS/pairwise potential.

α	DMC (10D)		DMC (Pairwise)		POS (Pairwise)
0.0001	4.230	+/-0.007	4.130	+/-0.007	4.156
0.001	39.78	+/-0.02	38.72	+/-0.01	38.93
0.01	262.6	+/-0.2	270.2	+/-0.1	270.8
0.1	1041	+/-2	1067	+/-2	1190
1	3653	+/-12	3583	+/-10	------

TABLE 4. Lowest five converged levels (J = 0,1,2) of each symmetry/nonzero statistical weight for a CH_5^+ n = 5 potential scaled by α. Energies are in cm^{-1} with residual convergence error (in parentheses) estimated as energy decrease with respect to the next smaller j_{max} basis set. By comparison with DMC results, the absolute energies for A_1^+ (J=0) are converged < 0.1 cm^{-1} and < 1 cm^{-1} for α = 0.01 and 0.01 respectively.

	J=0		J=1		J=2	
α	0.001	0.01	0.001	0.01	0.001	0.01
Γ						
	246.86 (0.02)	479.0 (1.7)	240.19 (0.29)	430.4 (18.1)	238.13 (0.24)	435.4 (19.2)
	322.08 (0.01)	545.0 (1.7)	327.76 (0.60)	553.6 (22.4)	244.33 (0.33)	484.7 (26.8)
A_2^+	375.57 (0.11)	609.6 (7.2)	349.42 (0.06)	572.6 (10.8)	322.43 (0.39)	517.3 (6.7)
	406.43 (0.20)	622.0 (7.7)	373.88 (0.24)	590.6 (15.3)	327.85 (0.48)	547.7 (45.2)
	425.34 (0.00)	630.1 (1.9)	375.02 (0.33)	600.9 (27.6)	340.42 (0.13)	560.8 (78.7)
	298.44 (0.01)	522.5 (3.0)	269.56 (0.25)	472.4 (15.4)	185.17 (0.46)	378.8 (32.5)
	325.38 (0.21)	551.7 (12.0)	292.05 (0.28)	486.0 (16.0)	289.83 (0.14)	481.4 (10.9)
A_2^-	406.30 (0.16)	632.5 (8.5)	323.56 (0.18)	548.9 (17.2)	296.19 (0.20)	521.2 (37.7)
	425.88 (0.11)	645.5 (9.8)	327.48 (0.13)	569.6 (9.9)		
	458.43 (0.37)	698.0 (15.1)	374.95 (0.34)	597.6 (26.1)		
	250.83 (0.03)	472.5 (1.9)	135.60 (0.03)	331.7 (4.2)	167.36 (0.45)	388.6 (21.1)
	255.60 (0.02)	498.5 (3.3)	163.77 (0.25)	373.3 (15.7)	214.69 (0.59)	432.2 (35.0)
G_2^+	306.40 (0.18)	546.8 (7.6)	220.12 (0.22)	427.5 (14.4)	239.70 (0.38)	451.4 (27.8)
	322.84 (0.02)	568.1 (3.8)	240.29 (0.21)	442.6 (15.4)	244.57 (0.58)	474.7 (40.0)
	329.75 (0.02)	583.1 (10.2)	241.92 (0.31)	448.6 (14.7)	245.48 (0.65)	489.1 (40.1)
	108.95 (0.04)	304.2 (3.1)	189.27 (0.17)	392.2 (10.7)	187.94 (0.62)	390.0 (35.1)
	192.39 (0.05)	399.0 (2.9)	197.61 (0.25)	432.8 (17.3)	190.88 (0.65)	411.6 (36.5)
G_2^-	216.28 (0.01)	425.4 (3.1)	221.84 (0.41)	440.2 (16.2)	192.94 (0.98)	423.7 (37.8)
	277.00 (0.04)	506.8 (2.6)	269.87 (0.29)	479.9 (15.3)	196.67 (0.93)	441.1 (29.5)
	280.09 (0.04)	527.7 (4.8)	271.25 (0.28)	482.4 (15.1)	216.75 (0.30)	452.6 (26.1)
	144.94 (0.08)	379.7 (5.7)	138.65 (0.05)	347.4 (9.4)	139.78 (1.07)	355.1 (43.9)
	173.88 (0.04)	410.1 (3.1)	163.11 (0.26)	374.1 (11.5)	166.38 (0.60)	397.9 (39.5)
H_2^+	217.60 (0.06)	464.4 (5.2)	171.42 (0.31)	403.0 (16.7)	169.84 (0.62)	406.6 (37.7)
	245.34 (0.03)	474.5 (2.6)	218.70 (0.18)	442.6 (10.9)	175.52 (0.81)	441.9 (33.5)
	253.30 (0.04)	496.5 (4.0)	221.80 (0.22)	447.4 (11.5)	217.08 (0.89)	443.1 (50.1)
	191.93 (0.05)	384.1 (1.8)	116.78 (0.05)	335.6 (5.2)	113.59 (1.01)	334.3 (46.3)
	198.73 (0.05)	422.3 (3.4)	162.66 (0.01)	382.5 (3.4)	190.62 (0.66)	404.2 (26.6)
H_2^-	214.81 (0.02)	458.1 (5.2)	190.46 (0.20)	402.8 (11.2)	191.94 (0.73)	425.1 (35.7)
	276.26 (0.05)	507.9 (1.4)	196.12 (0.29)	428.8 (22.4)	196.95 (1.03)	435.7 (36.2)
	279.29 (0.04)	509.5 (5.4)	200.71 (0.27)	442.3 (14.5)	198.97 (1.11)	441.8 (45.9)

TABLE 5. Expectation values of energy (in cm^{-1}) for a 1D X-H rotor in the pairwise potential corresponding to CH_5^+ $\alpha = 1$, demonstrating systematic convergence to the rigid body Diffusion Monte Carlo result (RBDMC) with increasing j_{max}.

j_{max}	$\langle E \rangle$ (cm^{-1})	Error
1	13104.0	371.8%
2	11278.2	306.0%
3	4638.3	67.0%
4	3644.0	31.2%
5	4543.5	63.6%
6	3322.0	19.6%
7	3019.0	8.7%
8	3097.7	11.5%
9	2820.5	1.5%
10	2783.7	0.2%
RBDMC	2777.7	

FIGURE CAPTIONS

Figure 1. Convergence behavior for a POS model of CH_4 ($\alpha = 1$, $J = 0$) as a function of j_{max}. The POS ground state energy is within 10 cm^{-1} of DMC predictions (dotted lines) by j_{max}=11.

Figure 2. POS convergence behavior for CH_4 ($\alpha = 0.033$) $J = 0, 1, 2, 3, 4$ energies as a function of j_{max}. The POS ground state (J=0) energy is compared against DMC predictions (dotted line).

Figure 3. a) CH_4 rotational energies of levels with $J = 0$ - 4 as a function of potential stiffness scale factor α. b) At higher resolution, centrifugal induced splittings of the nominally degenerate symmetric top levels for CH_4 are shown for $\alpha = 0.033$, which are considerably larger but match the qualitative patterns experimentally observed.

Figure 4. Bending energies of CH_4 as a function of the potential scale factor α.

Figure 5. Minimum energy paths for CH_5^+ through the C_s and C_{2v} transition states, separating the C_s minima. Note the remarkable agreement between critical points for the 10D relaxed potential and the pairwise fit.

Figure 6. Pair correlation functions for J=0 for CH_5 from DMC calculations for a series of potential models: a) 15D full CH_5^+ potential, b) the 10D relaxed potential, and c) the pairwise-additive least-squares fit.

Figure 7. Convergence of results for a POS CH_5^+ potential ($\alpha = 1$) $J = 0$ as a function of j_{max}. Though convergence in j_{max} is clearly indicated, the POS ground state is still appreciably higher than the DMC predictions (dotted lines). CPU times for each of the j_{max} values are also listed.

Figure 8. Ground-state energies of CH_5^+ as a function of the potential stiffness α, calculated by DMC and POS with both the 10D (DMC, open squares) and pairwise (POS, dashed line) potentials. The inset demonstrates level of convergence of POS and DMC (pairwise) calculations as a function of α. Note the excellent agreement between 10D and pairwise DMC calculations, further highlighting the surprising accuracy of the pairwise-additive potential approximation.

Figure 9. The lowest CH_5^+ $J = 0$ eigenenergies (with respect to the G_2^- ground state) as a function of potential stiffness ($\alpha = 0.0001$ to $\alpha = 0.1$) for each nuclear spin symmetry with non-zero statistical weight (results for all symmetries available on EPAPS.)
The trends in the POS energy level patterns indicate a noteworthy *absence* of tunneling splitting behavior with increasing α. This differs from Rotation-Contortion model results of Bunker and coworkers[59,61,80] (rightmost column), but is consistent with the delocalized wavefunctions, large zero-point energies, and small interconversion barriers inferred from DMC studies of McCoy, Bowman and coworkers.[45,76,79]

Figure 10. a) DMC pair correlation function of CH_5^+ as a function of α. b) Successive fits of the $\alpha = 1$ pair correlation function of CH_5^+ to a sum of Legendre functions. Such behavior suggests good convergence for the POS model of CH_5^+ by $j_{max} \approx 9$.

FIGURE 1

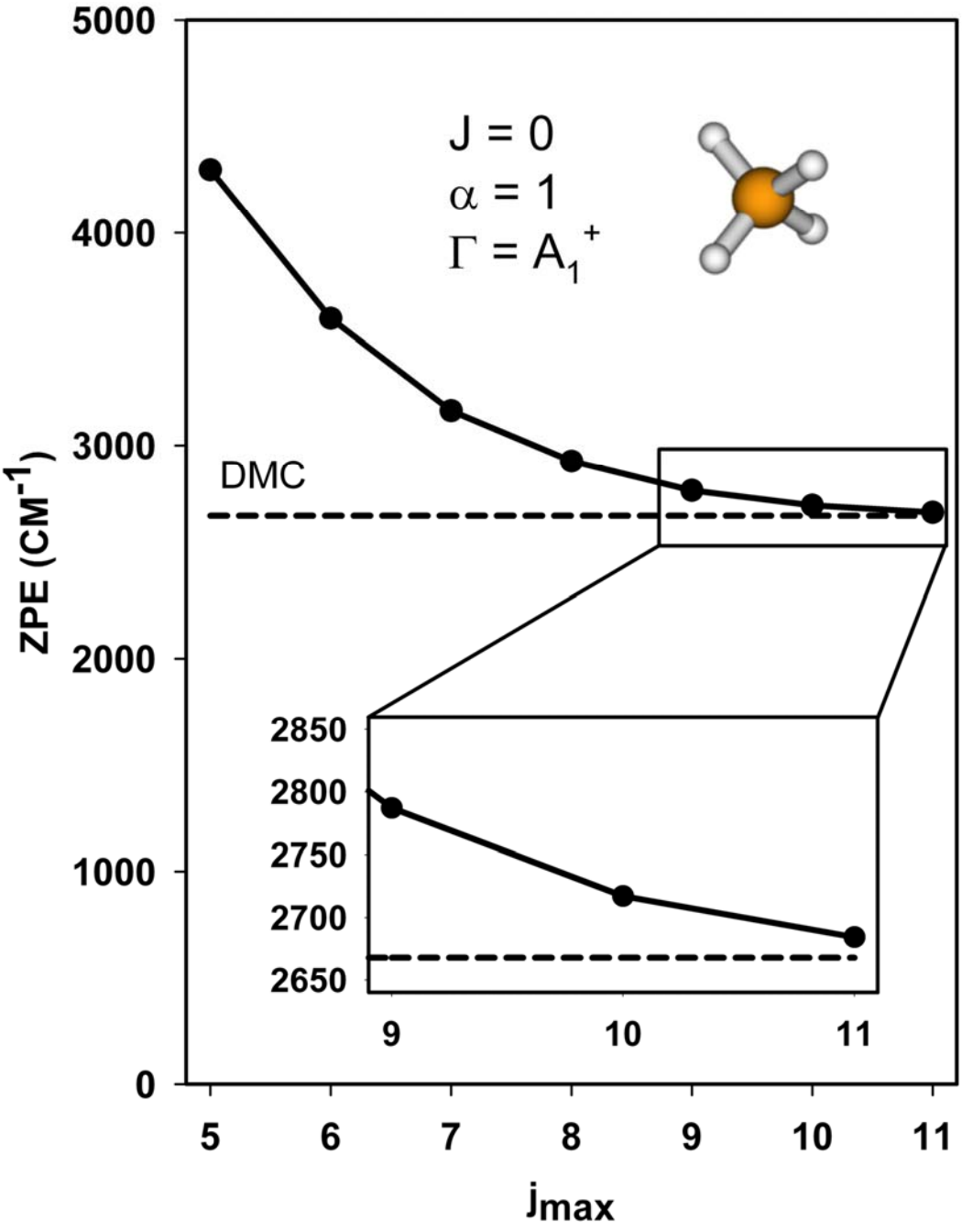
J = 0
α = 1
Γ = A1+
DMC
ZPE (CM-1)
5000
4000
3000
2000
1000
0
2850
2800
2750
2700
2650
9
10
11
5
6
7
8
9
10
11
jmax

FIGURE 2

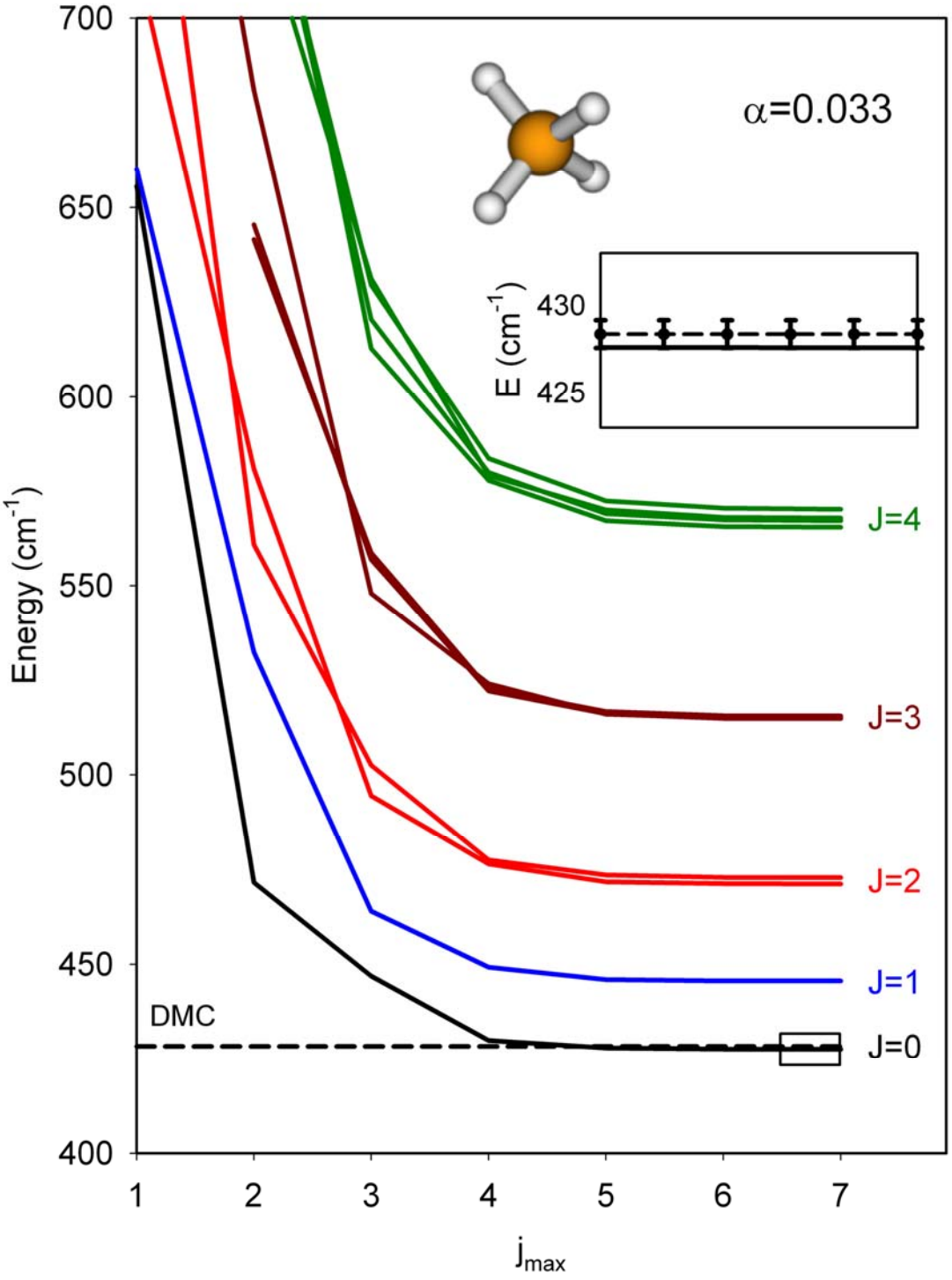
700
650
600
550
500
450
400
Energy (cm-1)
1
2
3
4
5
6
7
jmax
α=0.033
E (cm-1)
430
425
J=4
J=3
J=2
J=1
J=0
DMC

FIGURE 3

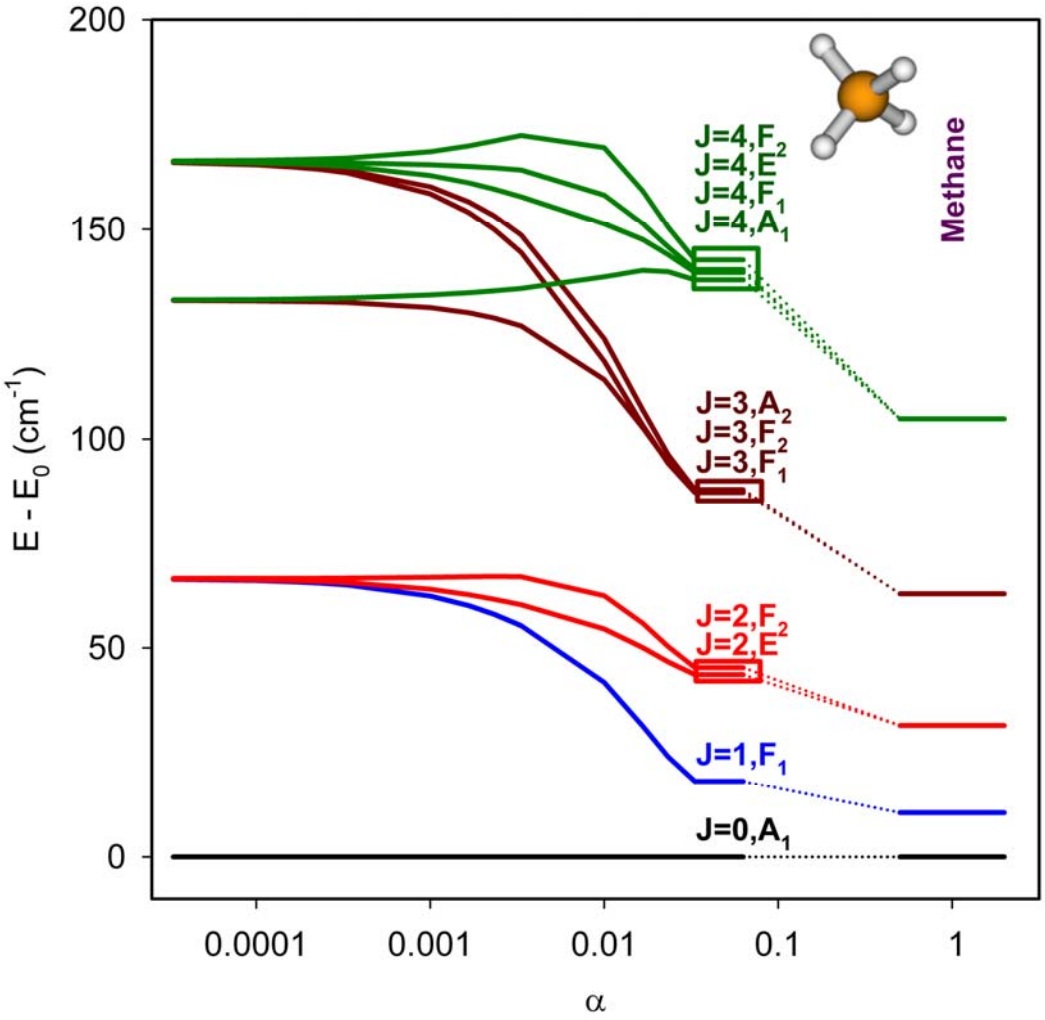
200
150
100
50
0
E - E0 (cm-1)
0.0001
0.001
0.01
0.1
1
α
J=4,F2
J=4,E
J=4,F1
J=4,A1
J=3,A2
J=3,F2
J=3,F1
J=2,F2
J=2,E
J=1,F1
J=0,A1
Methane

FIGURE 4

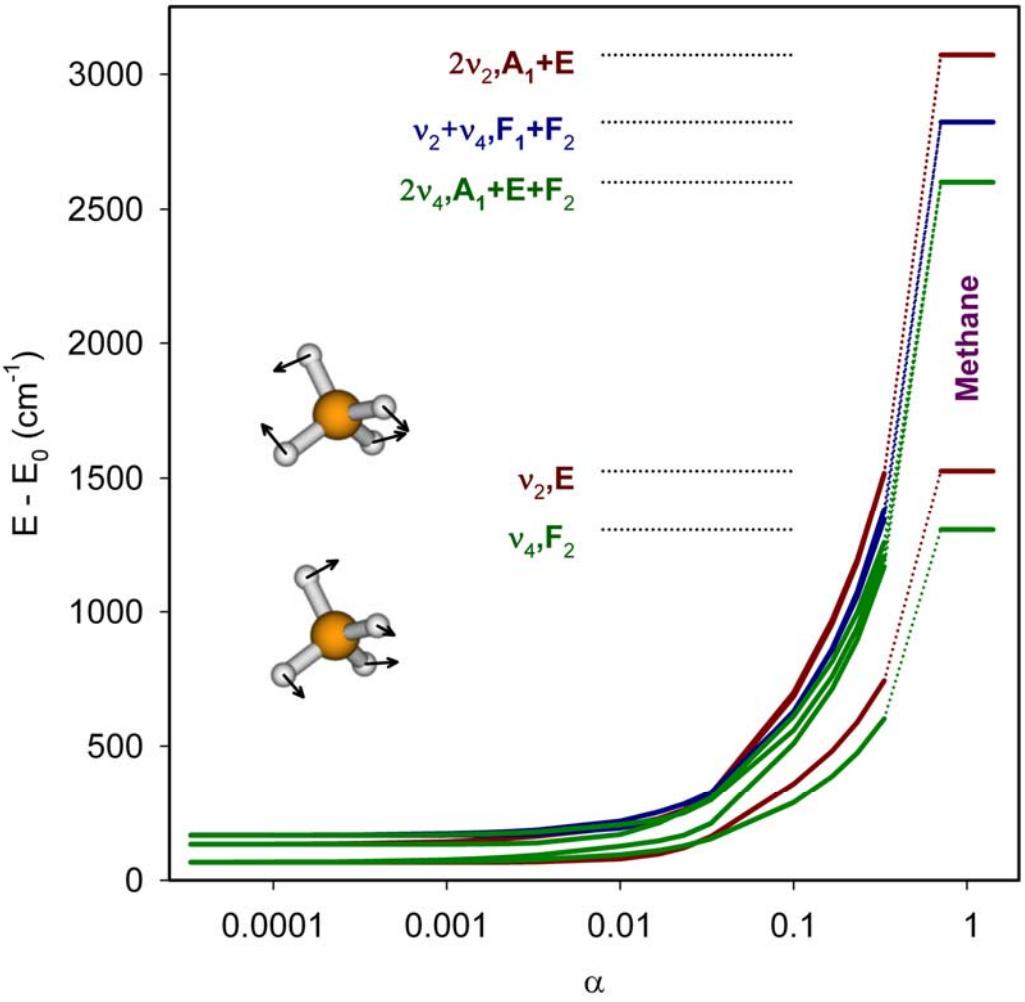
3000
2500
2000
1500
1000
500
0
E - E0 (cm-1)
0.0001
0.001
0.01
0.1
1
α
2ν2,A1+E
ν2+ν4,F1+F2
2ν4,A1+E+F2
ν2,E
ν4,F2
Methane

FIGURE 5

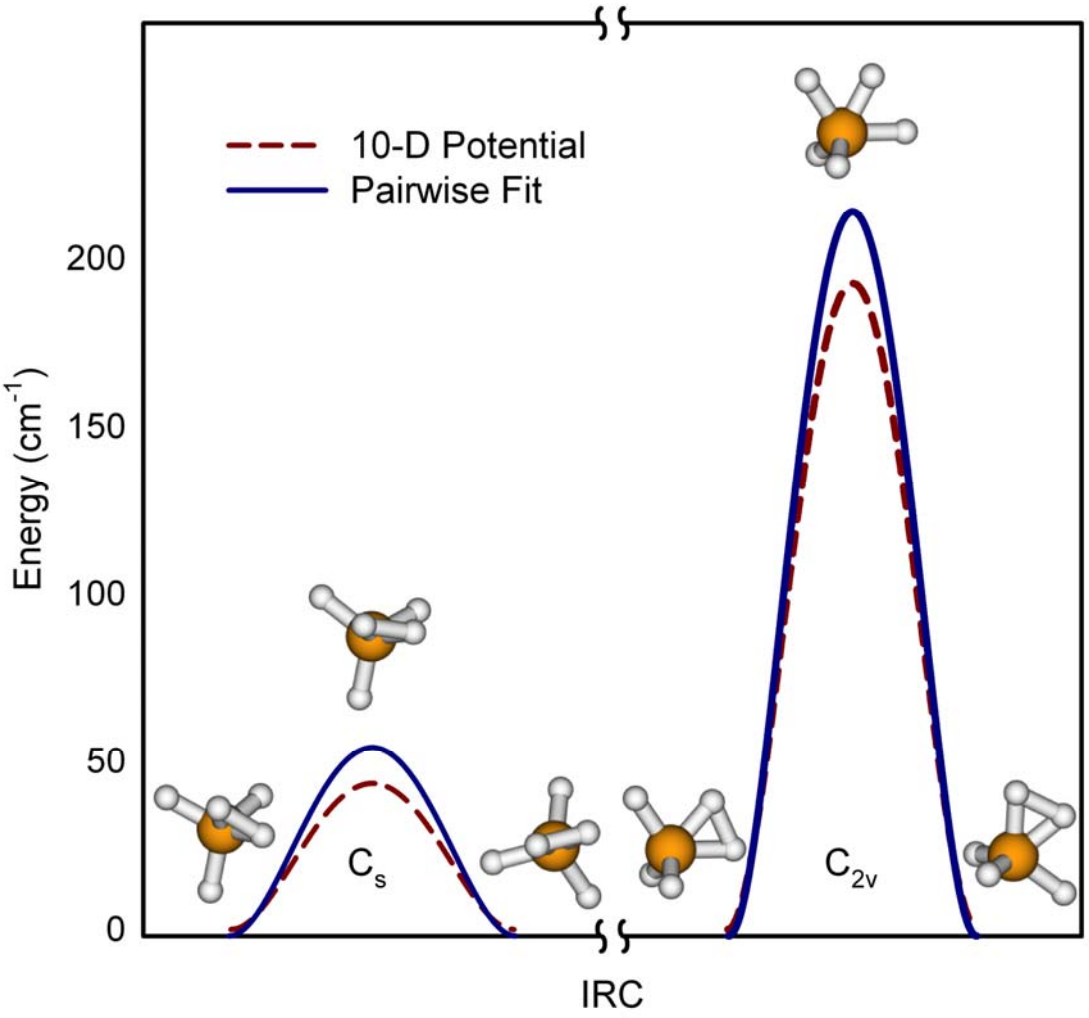
10-D Potential
Pairwise Fit
Energy (cm-1)
200
150
100
50
0
Cs
C2v
IRC

FIGURE 6

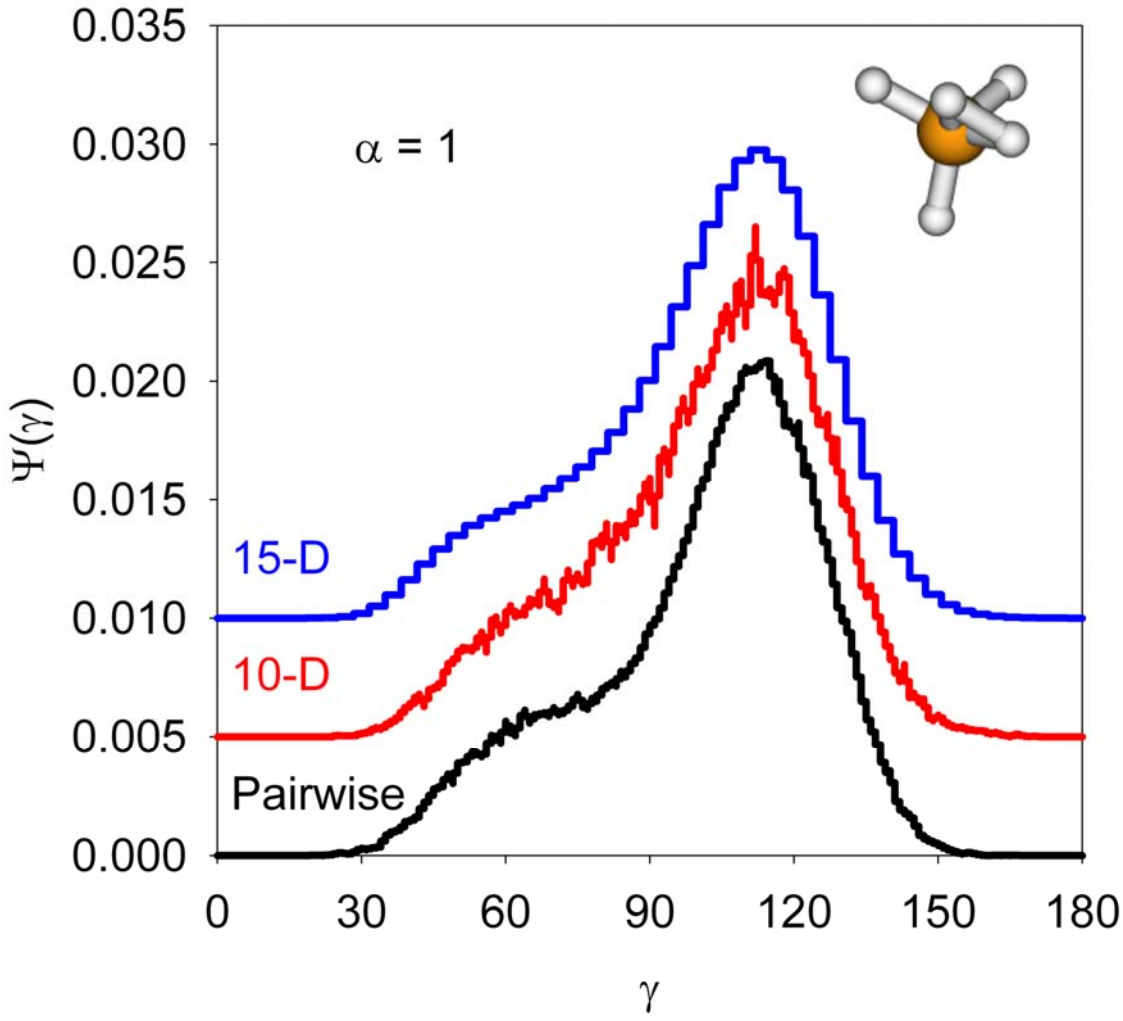
0.035
0.030
0.025
0.020
0.015
0.010
0.005
0.000
Ψ(γ)
α = 1
15-D
10-D
Pairwise
0
30
60
90
120
150
180
γ

FIGURE 7

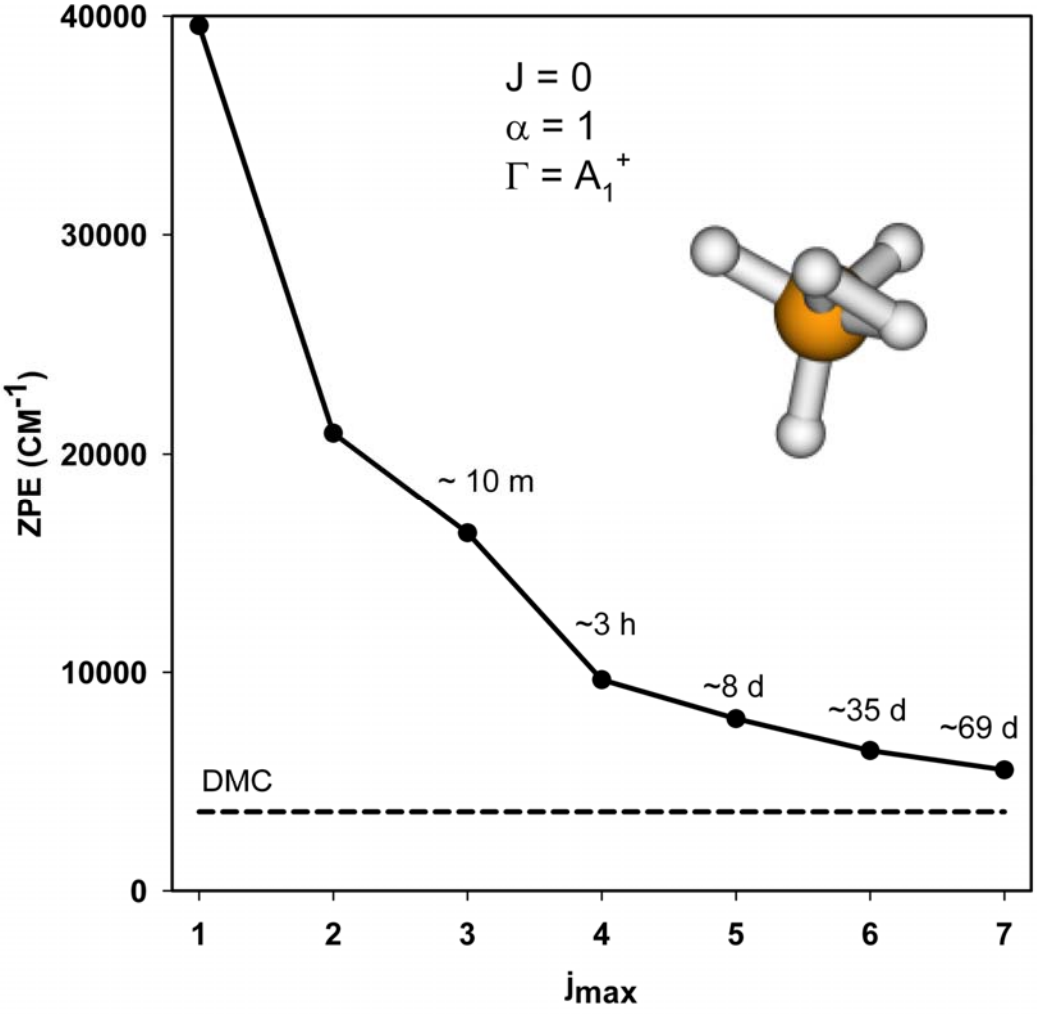
J = 0
α = 1
Γ = A1+
~ 10 m
~3 h
~8 d
~35 d
~69 d
DMC
ZPE (CM-1)
40000
30000
20000
10000
0
1
2
3
4
5
6
7
jmax

FIGURE 8

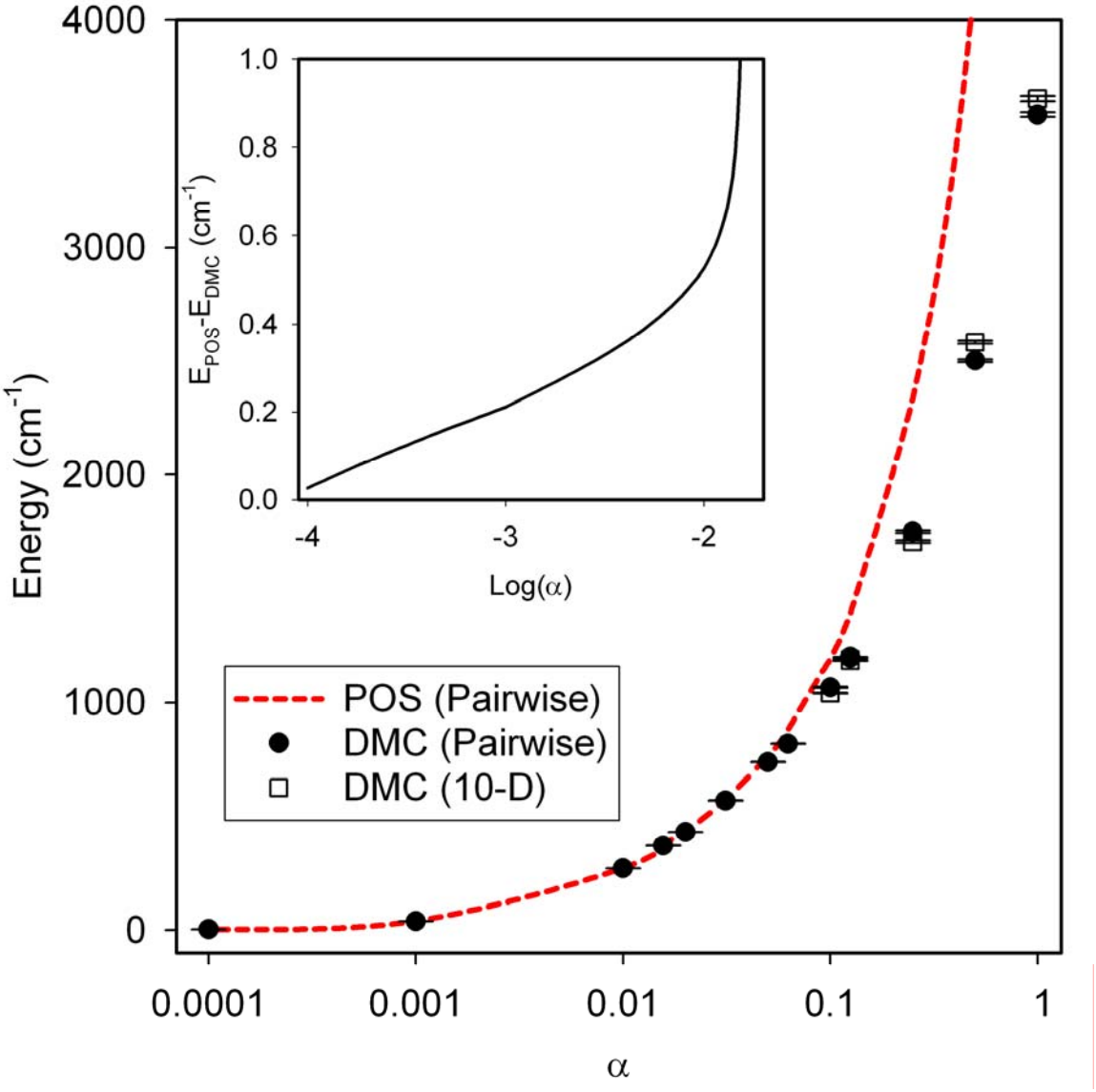
4000
3000
2000
1000
0
Energy (cm-1)
0.0001
0.001
0.01
0.1
1
α
POS (Pairwise)
DMC (Pairwise)
DMC (10-D)
1.0
0.8
0.6
0.4
0.2
0.0
EPOS-EDMC (cm-1)
-4
-3
-2
Log(α)

FIGURE 9

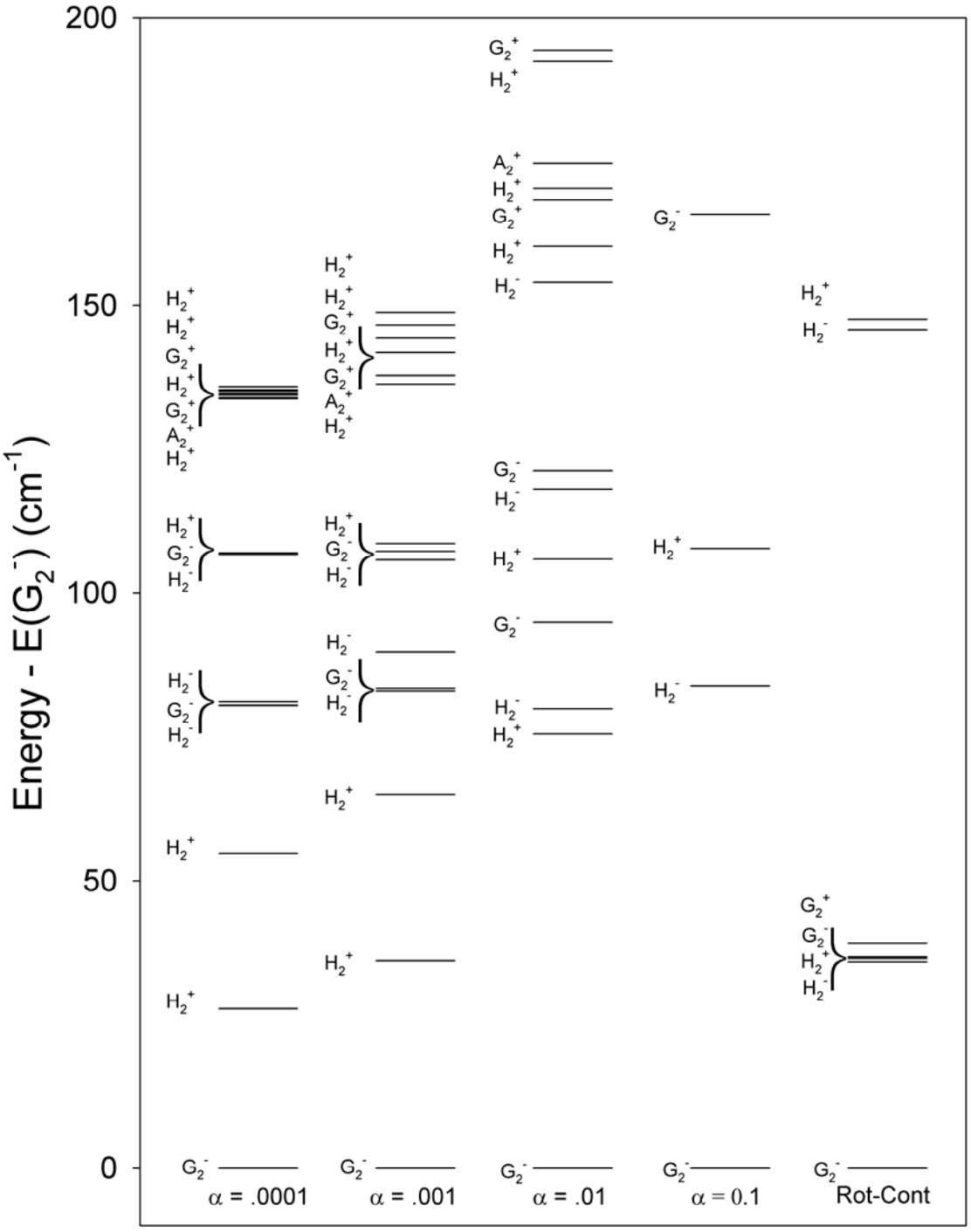

FIGURE 10

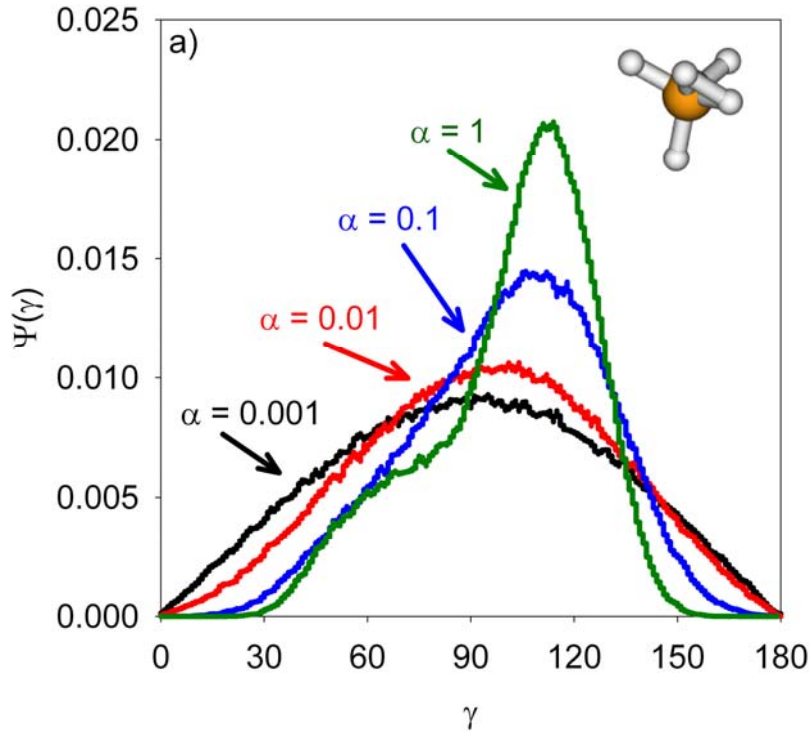
a)
α = 1
α = 0.1
α = 0.01
α = 0.001
Ψ(γ)
γ
0.025
0.020
0.015
0.010
0.005
0.000
0
30
60
90
120
150
180

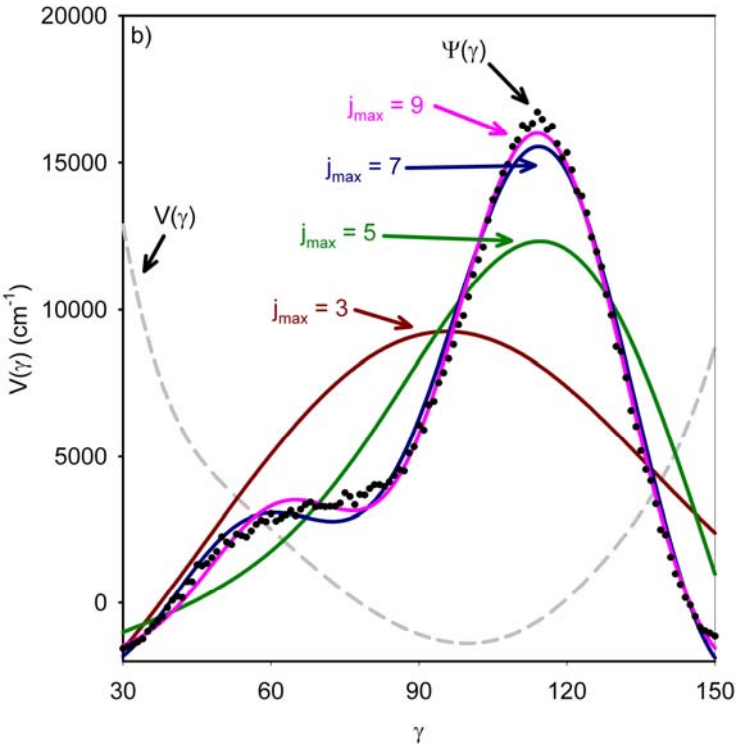
b)
Ψ(γ)
j_max = 9
j_max = 7
j_max = 5
j_max = 3
V(γ)
V(γ) (cm⁻¹)
γ
20000
15000
10000
5000
0
30
60
90
120
150